Thermochimica Acta, 233 (1994) 231–242
Elsevier Science B.V., Amsterdam
SSDI 0040-6031(93)01467-H

Thermal decomposition of magnesium citrate 14-hydrate

Seham A.A. Mansour

Chemistry Department, Faculty of Science, Minia University, El-Minia (Egypt)

(Received 27 May 1993; accepted 15 June 1993)

Abstract

Magnesium citrate 14-hydrate dehydrates endothermically on heating giving rise to the nanohydrate intermediate at 200°C. On further heating the anhydrous magnesium citrate is then formed and instantaneously loses two more moles of water forming magnesium aconitate which then decomposes to magnesium carbonate and finaly to magneisum oxide. The decomposition course has been monitored by TG, DTA and DSC measurements from which the non-isothermal kinetic and thermodynamic parameters have been determined. The decomposition processes have been characterized by analysing the decomposition products from each process using spectroscopy and X-ray diffractometry. The morphological and textural changes accompanying the decomposition processes have been examined by scanning electron microscopy.

INTRODUCTION

The thermal decomposition of several organic acid salts of alkaline earth metals (e.g. oxalates, acetates and formates), has been studied extensively [1]. However, a review of the literature [1–4] revealed little information on the decomposition behaviour of citrates. Continuing the study of citrate decomposition begun in relation to the thermal decomposition of bismuth citrate [5] and calcium citrate [6], the present paper attempts to clarify the stages encountered throughout the thermal decomposition course of magneisum citrate. The thermal analysis data was supplemented by analytical results of IR spectroscopy and X-ray diffractometry (XRD) of the parent salt, the intermediate(s) and the final product. Scanning electron microscopic (SEM) examinations of these materials were carried out to follow the morphological and textural changes at the various decomposition stages.

EXPERIMENTAL

Magnesium citrate $Mg_3(C_6H_5O_7)_2 \cdot 14H_2O$ (MgCi) used in this investigation was an AR grade BDH product. In terms of the thermal analysis results (see below), decomposition solid products were obtained by calcination of the parent citrate at chosen temperatures for 2 h, in a still atmosphere of air, and then kept dry for further analysis.

The thermal analyses (TG, DTA and DSC) were carried out using a Shimadzu thermal analyzer, model 30H (Japan) at different heating rates ($\theta = 5$, 10, 20 and 50°C min^{-1}). TG and DTA were carried out under dynamic air (30 ml min^{-1}) while DSC curves were recorded under dynamic nitrogen atmosphere (30 ml min^{-1}). Non-isothermal kinetic and thermodynamic parameters were calculated from the effect of heating rate on the maximum temperatures of the decomposition steps [7–9] as described earlier [10].

Infrared spectra in the 4000–300 cm^{-1} range, were obtained for MgCi and its solid decomposition products using a Perkin-Elmer 580B double-beam spectrophotometer (UK). The spectra were taken from thin discs ($\leq$ 20 mg cm^{-2}) of KBr-supported test samples (<1 mass%) at a resolution of 5.3 cm^{-1}.

XRD patterns were recorded for MgCi and its decomposition products using a JSX-60 Jeol diffractometer (Japan) with Ni-filtered Cu Kα radiation ($\lambda = 1.542$ Å). The diffraction patterns (I/I_0 versus d-spacing (Å)) thus determined were matched with the relevant ASTM standards [11] for identification purposes.

A 35 CF scanning electron microscope was used to examine MgCi and its decomposition products. The samples were mounted on the support by clear adhesive and coated by an Au/Pd layer using a sputter coater to render charging. For each sample, many crystals were examined and only features identified as being typical, reproducible and significant were photographed.

RESULTS AND DISCUSSION

Heating MgCi ($Mg_3(C_6H_5O_7)_2 \cdot 14H_2O$) in dynamic atmosphere of air showed that it decomposes to magnesium oxide via four steps. The TG and DTA curves recorded at heating rates of 5–50°C min^{-1} are shown in Fig. 1. The following discussion will consider the TG and DTA data recorded at 10°C min^{-1}.

Characterization of the decomposition steps

Step I

Figure 1 shows that step I occurs endothermically in the temperature range 110–190°C, with accompanying mass loss of 12.5% from the original. The DTA curves indicate that this step involves two overlapping processes. A tentative observation shows that these two processes involve two successive mass loss steps, 2.5% and then 10% of the original mass. The IR spectra of the products from these two processes (Fig. 2) at 130 and 230°C show reduction in the intensities of the citrate bands with respect to those displayed by the original salt. XRD of the decomposition product at 230°C

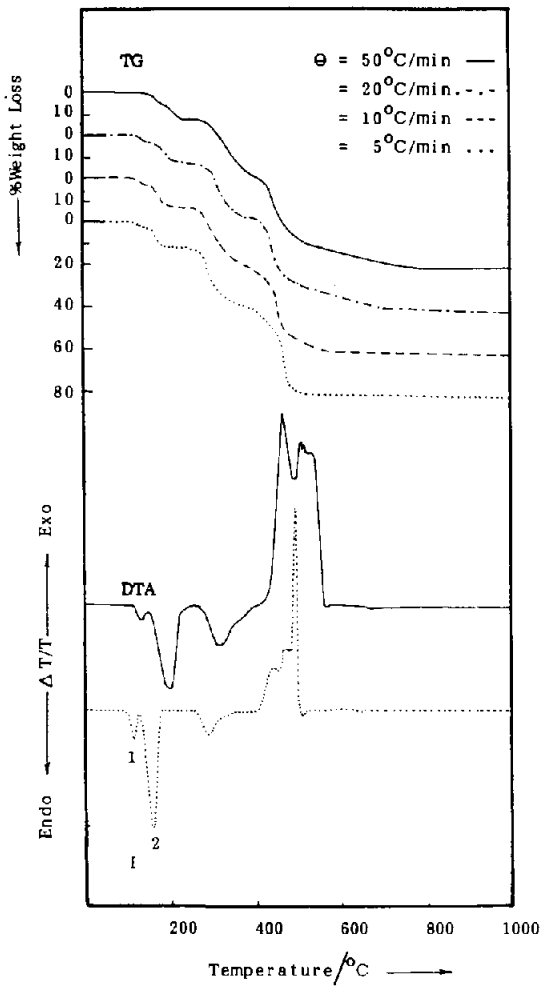

Fig. 1. TG and DTA curves recorded for MgCi at the heating rates θ indicated, in a dynamic (30 ml min^{-1}) air atmosphere.

shown in Fig. 3, reveals a diffractogram of an amorphous material. The corresponding mass losses of the two processes involved in this step (2.5 and 10% respectively) are very close to that calculated for the successive release of one and then four moles of water from MgCi.

$$\overbrace{Mg_3(C_6H_5O_7)_2 \cdot 14H_2O \xrightarrow[2.5\%]{1} \xrightarrow[10\%]{2} Mg_3(C_6H_5O_7)_2 \cdot 9H_2O}^{I}$$

The associated activation energies (ΔE) for these processes 1 and 2 were found to be equal, at 90 kJ mol^{-1} (Table 1).

Heating MgCi in the temperature range 110–190°C in dynamic N_2 flow resulted in thermal behaviour similar to that in air (Fig. 4), i.e. the commencement of the two endothermic dehydration processes 1 and 2.

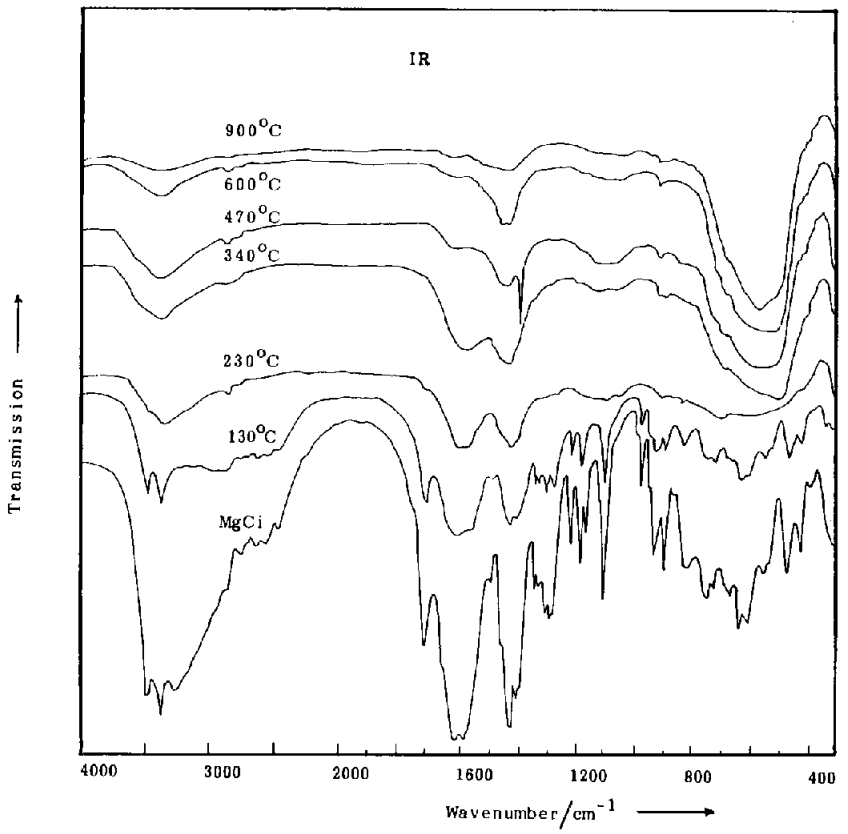

Fig. 2. IR spectra of MgCi and its decomposition products at the temperatures indicated for 2 h in still air.

These two processes also responded endothermically towards the DSC measurements in nitrogen atmosphere (Fig. 5) with activation energies (ΔE) of 121 and 97 kJ mol^{-1}, respectively (Table 2). The associated changes in enthalpy (ΔH) and entropy (ΔS) were found to be higher for the second process than for the first one (Table 2), indicating the increase in disorder accompanying dehydration step I. Hence, it could be concluded that the parent MgCi dehydrates through step I giving magnesium citrate nanohydrate as the intermediate.

Step II

Figure 1 indicates that step II occurs endothermically in the temperature range 260–350°C. The DTA curve shows that the corresponding peak has a small shoulder. The IR spectrum of the decomposition product at 340°C, near the end of this step, shows great similarity to that of the decomposition product at 230°C. The mass loss corresponding to this step is 27.5%, which brings the total loss up to 40% from the original mass. Such mass loss is

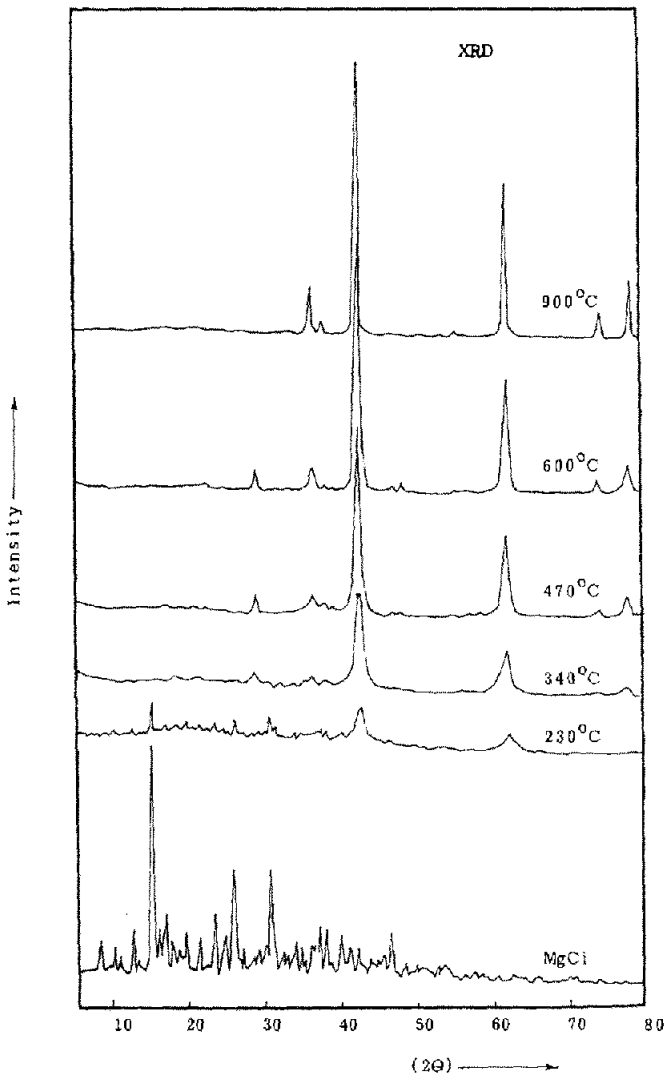

Fig. 3. XRD power diffractograms for MgCi and its decomposition products at the temperatures indicated for 2 h in still air.

higher than that calculated (35%) for the complete dehydration of MgCi. The extra mass loss tallies fairly well with that anticipated for the release of an extra two moles of water. Therefore, this step may reasonably involve the completion of the dehydration process of MgCi and then transformation of the anhydrous citrate to magnesium aconitate

$$Mg_3(C_6H_5O_7)_2 \cdot 9H_2O \xrightarrow[-11H_2O]{II} Mg_3(C_6H_3O_6)_2$$

The activation energy (ΔE) was found to be 129 kJ mol^{-1} (Table 1).

Figure 4 indicates that this second dehydration step also took place

TABLE 1

Non-isothermal kinetic parameters of the thermal steps encountered throughout the decomposition course of MgCi in air

Thermal step	T_{max} [a]	ΔE/kJ mol^{-1}	log A	k/min^{-1}	$\Delta T/T$
I 1	121	89	11	15×10^{2}	endo
2	176	90	9	23×10^{-2}	endo
II	302	129	10	12×10^{-2}	endo
III	452	400	29	46×10^{-2}	exo
IV	465	79	4	16×10^{-2}	exo

[a] Values obtained from TG curve recorded at 10°C min^{-1}.

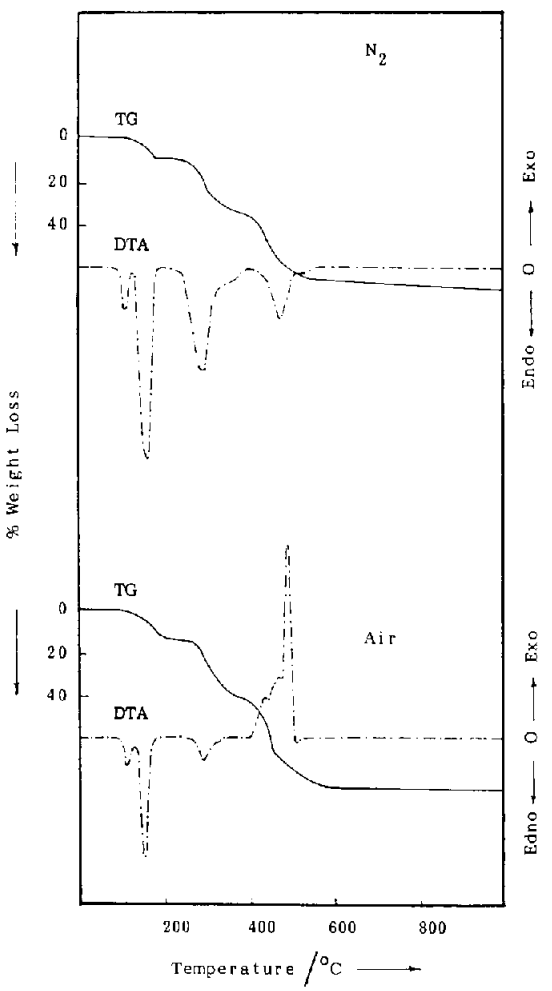

Fig. 4. TG and DTA curves recorded for MgCi at 10°C min^{-1}, in dynamic (30 ml min^{-1}) atmosphere of dry N_2 or air.

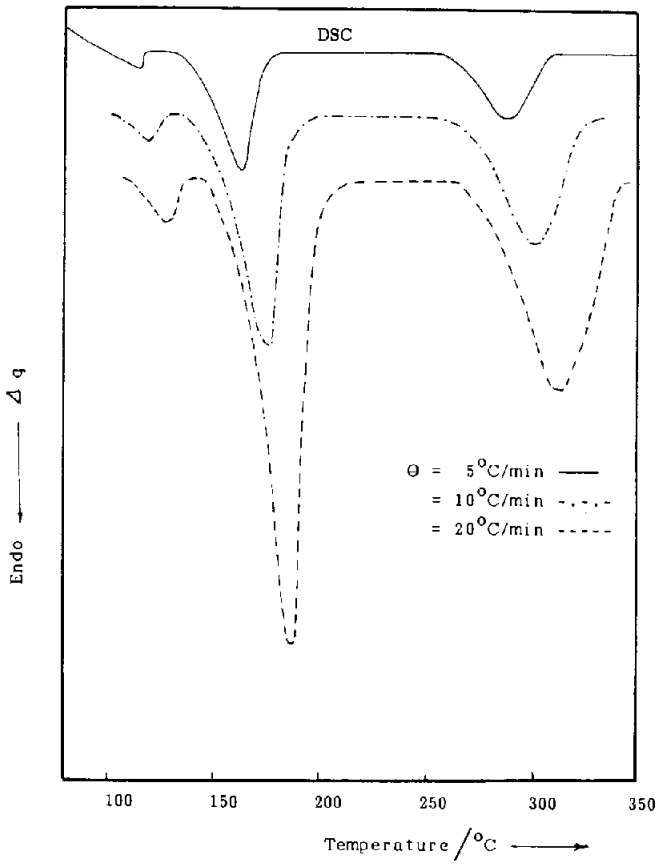

Fig. 5. DSC curves recorded for MgCi at the heating rates (θ) indicated in dynamic (30 ml min^{-1}) atmosphere of dry N_2.

TABLE 2

Non-isothermal kinetic and thermodynamic parameters of the thermal steps encountered throughout the decomposition course of MgCi in nitrogen, based on the recorded DSC curves

Thermal step	ΔE/kJ mol^{-1}	Ln A	k/min^{-1}	ΔH/kJ mol^{-1}	C_p/J g^{-1}	ΔS/J K^{-1} g^{-1}	$\Delta q/q$
I	121	36	0.93	9.9	0.83	0.51	endo
II	97	25	0.57	129.5	4.6	0.64	endo
III	149	30	0.54	109.06	3.4	0.39	endo

endothermically in nitrogen in the temperature range 250–390°C. The observed mass loss of 36% accompanying this process is very close to that calculated (about 35.8%) for the complete dehydration of the salt (i.e. the formation of anhydrous magnesium citrate). The DSC response of this process (Fig. 5) is endothermic showing a well formed peak, with associated energy of activation (ΔE) of 149 kJ mol^{-1} and an enthalpic change (ΔH) of 109 kJ mol^{-1} (Table 2). The decrease in the entropy change (ΔS) and the C_p values compared with that of the previous process (Table 2) indicates the decrease in the disorder accompanying the complete dehydration of the salt under nitrogen flow.

Steps III and IV

Figure 1 indicates that the decomposition of magnesium citrate is completed through two overlapping exothermic steps III and IV, with a corresponding mass loss of 42%, bringing the total loss up to 82% from the original mass. The figure indicates that these two steps are better resolved in the curves conducted at higher heating rates. The TG curves reveal that the material loses more than 20% of the original mass in a very narrow temperature range (about 50°C) while the completion of the decomposition extends over a wider range depending on the heating rate. A question arises here, as to whether step III involves complete decomposition of part of the salt (as occurs, for example, in the decomposition of ammonium perchlorate [1]), or partial decomposition of all of the salt to some intermediate (e.g. the decomposition of calcium oxalate to calcium oxide via the carbonate [12]).

The IR spectrum of the decomposition product at 470°C (Fig. 2) displays new bands at 877(s), 1070(w) and 1440(ms) cm^{-1}, which are assigned to magnesium carbonate [13]. The spectrum revealed the presence of $\rangle C{=}C\langle$ by displaying the C–H out-of-plane deformation mode absorption band at 970 cm^{-1} which slightly interfered with the band of the carbonate at 1070 cm^{-1}. The absorption bands of the carbonate are still displayed in the spectrum of the decomposition product at 600°C, while the IR spectrum of the decomposition product at 900°C exhibits nothing but the broad absorption band of MgO [14]. The XRD pattern (Fig. 3) of the decomposition product at 470°C shows strong lines which match well with the characteristic lines of MgO (ASTM card no. 4-829), in addition to very weak lines relevant to those of $MgCO_3$ (ASTM card no. 8-479). Figure 3 indicates the dominance of the MgO phase amongst the decomposition products at 600° and 900°C. It also reveals the increase in crystallinity with increase of calcination temperature. Hence, the following reactions could presumably be involved in steps III and IV

$$Mg_3(C_6H_3O_6)_2 \xrightarrow{III} 3MgCO_3 + 3H_2O + 9C$$

$$MgCO_3 \xrightarrow{IV} 3MgO + 3CO_2$$

The first reaction is obviously accompanied by the formation of elemental carbon which would undergo pyrolysis into CO and/or CO_2 with oxygen from the air flow, resulting in steps III and IV being exothermic in air. Such a pyrolysis process does not occur in nitrogen flow where oxygen is not available. In fact all the decomposition steps of MgCi are endothermic in dynamic atmosphere of dry nitrogen as is clear from Fig. 4.

Electron microscopy

Morphological and textural changes occurring during the decomposition course of MgCi were characterized by comparative examinations of scanning electron micrographs. SEM studies of the parent salt revealed that it is composed of well-formed, approximately tetragonal crystals with smooth surfaces and sharp edges which are of narrow size-range (Fig. 6(a)). Occasional twinning and some aggregates of crystallites were observed (Fig. 6(b)). Many of the larger crystallites included smaller crystals embedded in their surfaces and some crystals were apparently slightly damaged. Heating up to 130°C resulted in the appearance of a slight splintering due to mechanical disruption (Fig. 7) which represents the start of the dehydration process. The splintering in this early dehydration stage occurred predominantly parallel to the major axis of the crystals, but later on, for the samples heated at 340°C, the cleaves became more random (Fig. 8(a)). The electron micrographs at this temperature revealed large areas of apparently unaltered crystallite surfaces, as is clear from Fig. 8(b). These crystallites have, however, already undergone dehydration and the only feature was the presence of some cracks on the surface (Fig. 8 (a, b)). The electron micrographs of the samples heated to 470°C revealed an alteration of crystallite texture. Figure 9 showed that the decomposition developed in the cleaves and then proceeded in all directions, giving rise to a material of indeterminate structure. The micrograph shows the presence of another crystallite shape. These results are in accordance with the proposed decomposition scheme where dehydration is completed before decomposition starts, and that at 470°C there is a minute portion of $MgCO_3$ in addition to the main product MgO.

CONCLUSIONS

From the results obtained the following conclusions may be drawn:

(1) The dehydration of $Mg_3(C_6H_5O_7)_2 \cdot 14H_2O$ takes place in three endothermic processes, the first two of which overlap.

(2) The only observed textural feature after completion of the dehydration processes is the splintering of the crystal surfaces.

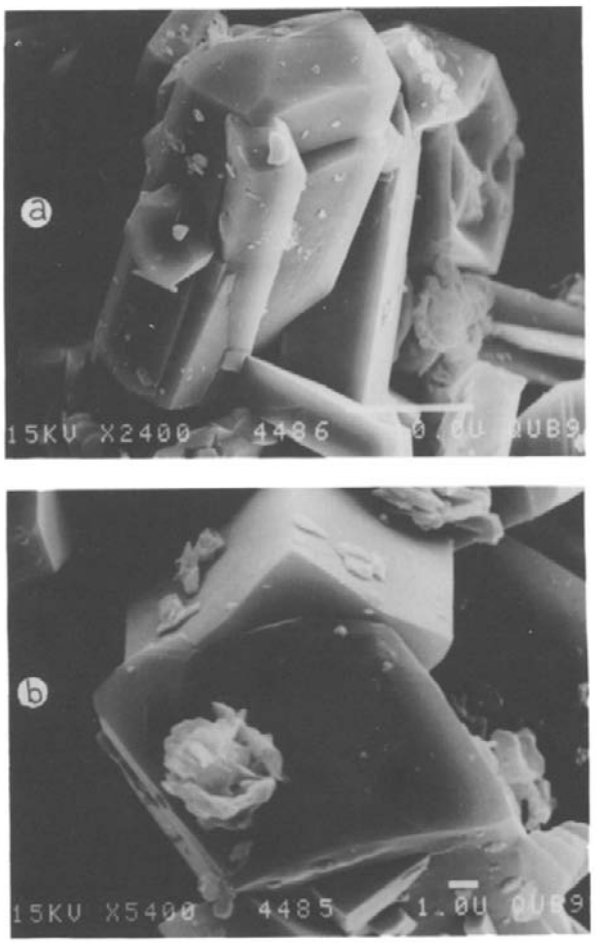

Fig. 6. Scanning electron micrographs of the parent MgCi, showing (a) collection of well-formed crystals, (b) of tetragonal appearance with smooth surfaces.

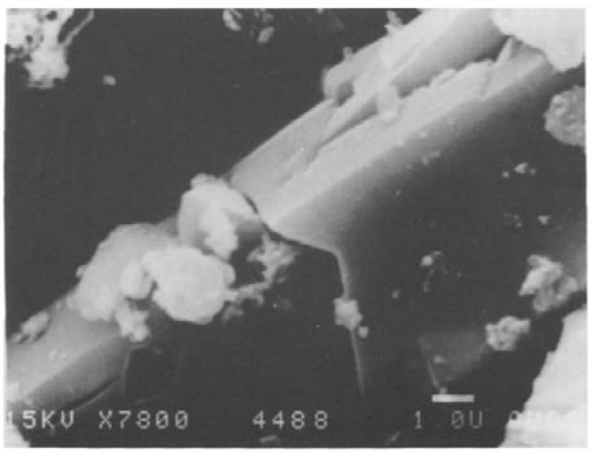

Fig. 7. Scanning electron micrograph of the decomposition product at 130°C.

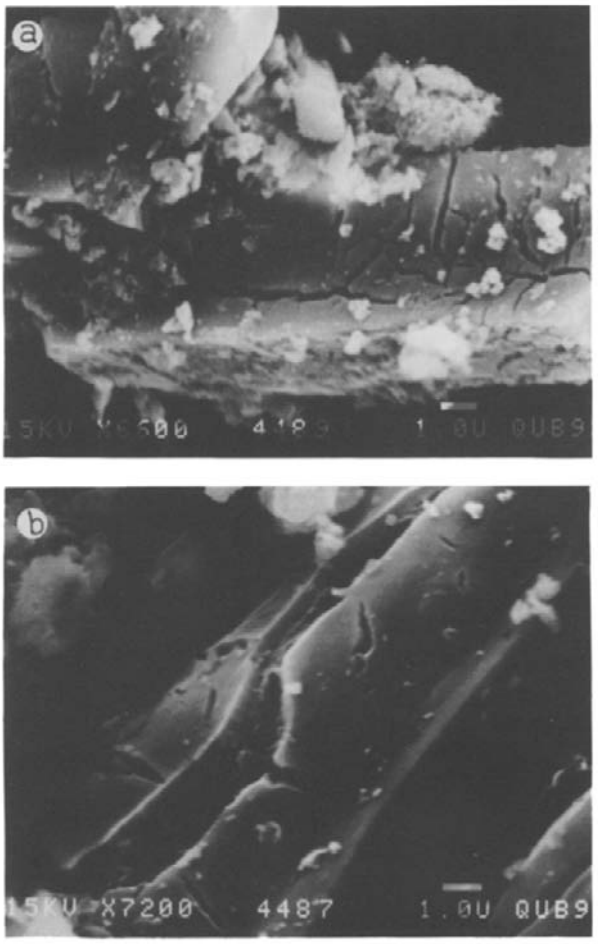

Fig. 8. Scanning electron micrographs of the decomposition product at 340°C, revealing (a) the random splintering of the surface and (b) the presence of areas of unaltered crystallite surfaces.

(3) Decomposition then occurs through two overlapping processes which take place exothermically in dynamic air and endothermically in flowing nitrogen.

(4) The thermal decomposition of magnesium citrate 14-hydrate may involve the following pathways

$$\overbrace{\mathrm{Mg_3(C_6H_5O_7)_2 \cdot 14H_2O \xrightarrow[2.5\%]{1} \xrightarrow[10\%]{2}}}^{\mathrm{I}} \mathrm{Mg_3(C_6H_5O_7)_2 \cdot 9H_2O \xrightarrow[11H_2O]{II}}$$

$$\mathrm{Mg_3(C_6H_3O_6)_2 \xrightarrow[-3H_2O]{III} 3MgCO_3 \xrightarrow[-3CO_2]{IV} 3MgO}$$

$$-9\mathrm{C\ (as\ CO\ and/or\ CO_2)}$$

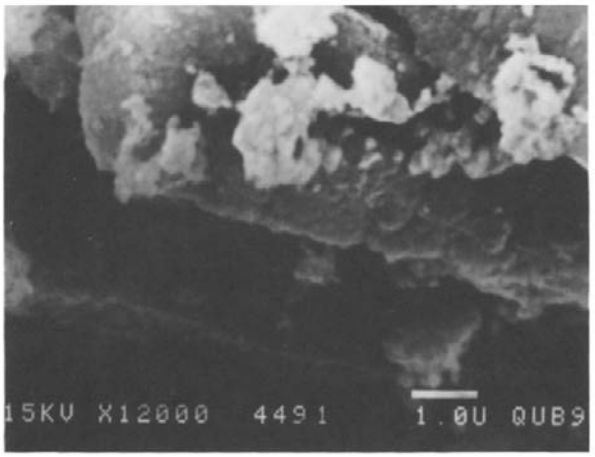

Fig. 9. Scanning electron micrograph of the decomposition product at 470°C.

ACKNOWLEDGEMENTS

It is a pleasure to thank the Queen's University of Belfast, particularly the staff of the electron microscope for assistance in obtaining the electron micrographs. Thanks are also due to the Egyptian Government for the grant of a fellowship.

REFERENCES

1 M.E. Brown, D. Dollimore and A.K. Galwey, Comprehensive Chemical Kinetics, Vol. 22. Reactions in the Solid State, Elsevier, Amsterdam, 1980.
2 A. Srivastava, P. Singh, V.G. Gunjikar and C.I. Jose, Thermochim. Acta, 76 (1984) 249.
3 J. Mastowska, J. Therm. Anal., 29 (1984) 895.
4 J. Mastowska, M. Bielawski and A. Baranowska, Thermochim. Acta, 92 (1985) 235.
5 S.A.A. Mansour, Thermochim. Acta, 233 (1994) 257.
6 S.A.A. Mansour, Thermochim. Acta, 233 (1994) 243.
7 T. Ozawa, J. Therm. Anal., 2 (1970) 301.
8 K.F. Baker, Du Pont Instruments, Thermal Analysis Application Brief No. TA-53.
9 C. Heald and A.C.K. Smith, Applied Physical Chemistry, Macmillan, London, 1982, pp. 20–40.
10 S.A.A. Mansour, Thermochim. Acta, 228 (1993) 155.
11 W. Frank et al. (Eds.), Powder Diffraction File for Inorganic Phase, Int. Center for Diffraction Data, Philadelphia, PA, 1981.
12 D.A. Young, Decomposition of Solids. Pergamon, Oxford, 1966.
13 J.A. Gadsden, Infrared Spectra of Minerals and Related Inorganic Compounds, Butterworths, London, 1975, p. 64.
14 F.F. Bentley, L.D. Smithson and A.L. Rozek, Infrared Spectra and Characteristic Frequencies ≈700–300 cm^{-1}, Wiley, New York, 1968, p. 1535.